Title

Increased lateral microtubule contact at the cell cortex is sufficient to drive mammalian spindle elongation.

Journal

Molecular biology of the cell, 28(14)

ISSN

1059-1524

Authors

Guild, Joshua
Ginzberg, Miriam B
Hueschen, Christina L
et al.

Publication Date

2017-07-01

DOI

10.1091/mbc.e17-03-0171

Peer reviewed

Increased lateral microtubule contact at the cell cortex is sufficient to drive mammalian spindle elongation

Joshua Guild[a], Miriam B. Ginzberg[b,c], Christina L. Hueschen[a,d], Timothy J. Mitchison[b], and Sophie Dumont[a,d,e,*]

[a]Department of Cell and Tissue Biology and [d]Biomedical Sciences Graduate Program, University of California, San Francisco, San Francisco, CA 94131; [b]Department of Systems Biology, Harvard Medical School, Boston, MA 02115; [c]The Hospital for Sick Children, Toronto, ON M5G 1X8, Canada; [e]Department of Cellular and Molecular Pharmacology, University of California, San Francisco, San Francisco, CA 94143

ABSTRACT **The spindle is a dynamic structure that changes its architecture and size in response to biochemical and physical cues. For example, a simple physical change, cell confinement, can trigger centrosome separation and increase spindle steady-state length at metaphase. How this occurs is not understood, and is the question we pose here. We find that metaphase and anaphase spindles elongate at the same rate when confined, suggesting that similar elongation forces can be generated independent of biochemical and spindle structural differences. Furthermore, this elongation does not require bipolar spindle architecture or dynamic microtubules. Rather, confinement increases numbers of astral microtubules laterally contacting the cortex, shifting contact geometry from "end-on" to "side-on." Astral microtubules engage cortically anchored motors along their length, as demonstrated by outward sliding and buckling after ablation-mediated release from the centrosome. We show that dynein is required for confinement-induced spindle elongation, and both chemical and physical centrosome removal demonstrate that astral microtubules are required for such spindle elongation and its maintenance. Together the data suggest that promoting lateral cortex–microtubule contacts increases dynein-mediated force generation and is sufficient to drive spindle elongation. More broadly, changes in microtubule-to-cortex contact geometry could offer a mechanism for translating changes in cell shape into dramatic intracellular remodeling.**

Monitoring Editor
Samara Reck-Peterson
University of California, San Diego

Received: Mar 17, 2017
Revised: Apr 28, 2017
Accepted: Apr 28, 2017

INTRODUCTION

Over the course of mitosis, the microtubule-based spindle remakes and remodels itself, morphing in shape to fulfill the needs of each mitotic stage. The prometaphase spindle captures and moves chromosomes, ultimately reaching a steady state—the metaphase spindle—with a central plate of aligned chromosomes. At anaphase, astral microtubules lengthen as the spindle elongates dramatically and reels in chromatids to its two poles, ensuring their separation into daughter cells. At telophase and cytokinesis, the spindle reorganizes itself again, developing a prominent midzone structure that directs furrow ingression and abscission.

Changes in spindle length are a striking example of the spindle's ability to remodel itself in response to biochemical and physical cues. For example, anaphase onset triggers spindle elongation, and the metaphase spindle dramatically increases its steady-state length in response to a simple physical cue, cell confinement (Dumont and Mitchison, 2009a; Lancaster *et al.*, 2013). What factors regulate such spindle remodeling, and how are physical cues like confinement sensed? In *Caenorhabditis elegans* and mammals, cortical dynein pulling on astral microtubules—and therefore on centrosomes—is an important factor for anaphase B spindle elongation (Aist *et al.*, 1993; O'Connell and Wang, 2000; Grill *et al.*, 2001, 2003; Labbe *et al.*, 2004; Krueger *et al.*, 2010;

This article was published online ahead of print in MBoC in Press (http://www.molbiolcell.org/cgi/doi/10.1091/mbc.E17-03-0171) on May 3, 2017.

J.G., M.B.G., C.L.H., and S.D. conceived and designed experiments; J.G. and M.B.G. performed the experiments; J.G., M.B.G., C.L.H., T.J.M., and S.D. analyzed the data; J.G. prepared the digital images; and J.G., C.L.H., and S.D. drafted the article.

*Address correspondence to: Sophie Dumont (sophie.dumont@ucsf.edu).

Abbreviations used: GFP, green fluorescent protein; k-fiber, kinetochore-fiber; PDMS, polydimethylsiloxane.

Collins *et al.*, 2012; Kiyomitsu and Cheeseman, 2013; Wu *et al.*, 2016). In metaphase, cortical dynein pulling forces are also present (Nguyen-Ngoc *et al.*, 2007; Kiyomitsu and Cheeseman, 2012; Kotak *et al.*, 2012), but sister chromatid decoupling is not sufficient to induce spindle elongation (Zhang and Nicklas, 1996; Brennan *et al.*, 2007).

Recent work suggests that microtubule contact geometry ("end-on" vs. lateral) at the cell cortex may be a governing parameter of cortical force generation. Cortically anchored motors can either capture microtubule tips end-on to harness energy from microtubule depolymerization, or they can slide astral microtubules laterally against the cortex to generate pulling force "side-on" (Adames and Cooper, 2000; Tsou *et al.*, 2003; Fink *et al.*, 2006; Kozlowski *et al.*, 2007; Gusnowski and Srayko, 2011; Laan *et al.*, 2012). In mammalian metaphase cells, depleting microtubule-associated proteins that normally facilitate end-on capture leads to highly persistent lateral contacts that misposition the spindle (Samora *et al.*, 2011; Kern *et al.*, 2016). In *C. elegans*, promoting more lateral microtubule growth against the cell cortex increases the rate of anaphase B spindle elongation (O'Rourke *et al.*, 2010), suggesting that force scales with the extent of lateral contact. Careful observation of astral microtubules in mammalian cells reveals that end-on to side-on contact geometry transitions increase as the spindle begins to lengthen at anaphase onset (Kwon *et al.*, 2015). Together these data hint at a functional connection between cortical microtubule contact geometry and spindle elongation.

Here we test the hypothesis that changes in microtubule contact geometry can induce spindle elongation in mammalian cells. We use physical perturbations to change cell shape and spindle architecture and to probe force regulation in real time. A key strength of this approach is its isolation of the effect of mechanical inputs, independent of biochemical regulation (Su *et al.*, 2016). Given that cell confinement induces metaphase spindle elongation via an unknown mechanism (Dumont and Mitchison, 2009a; Lancaster *et al.*, 2013), we wondered whether confinement regulates astral microtubule-to-cortex contact geometry and, if so, whether changes in contact geometry are sufficient to trigger spindle elongation. We combined dynamic cell confinement with laser ablation and found that confinement drives spindle elongation and that this does not require bipolar spindle architecture, dynamic microtubules, or an anaphase cytoplasm. Instead, confinement promotes lateral astral microtubule contact geometries at the cell cortex, where cortical sliding forces are present at metaphase. Furthermore, both dynein-powered force generation and astral microtubules are required for confinement-induced spindle elongation in metaphase. Together the data support a model in which increasing lateral microtubule contacts at the cortex is sufficient to drive spindle elongation in mammals. Moreover, this study contributes to our understanding of how cell shape and size can regulate intracellular organization (Thery *et al.*, 2007; Wuhr *et al.*, 2010; Fink *et al.*, 2011; Kimura and Kimura, 2011; Minc *et al.*, 2011).

RESULTS AND DISCUSSION

Metaphase, anaphase, monopolar, and Taxol-stabilized spindles elongate at similar rates when confined

To test a functional connection between astral microtubule-to-cortex contact geometry and mammalian spindle elongation, we aimed to physically change contact geometry and test whether it correlated with spindle elongation. Because cell confinement changes cell shape and leads the spindle to elongate and reach a new steady-state length, this seemed to be a reasonable approach. If confinement does drive spindle elongation through cortical-contact geometry changes, changes in forces from outside—rather than inside—the spindle should trigger spindle elongation. To test this, we reproducibly confined PtK2 cells using polydimethylsiloxane (PDMS)-based devices (Le Berre *et al.*, 2012) and mapped the elongation responses of spindles with modified force-generation mechanisms inside the spindle. The devices reduced cell height in a highly reproducible manner, bringing metaphase cells from an unconfined height of 9.2 ± 0.5 µm (n = 8) to a confined height of 3.1 ± 0.2 µm (n = 8) (Figure 1A and Supplemental Video 1).

First, we tested whether metaphase and anaphase spindles—which have different architectures and biochemistries—have different spindle elongation potentials under confinement. Confinement led to indistinguishable (p = 0.84) rates of spindle elongation at metaphase and anaphase B: the spindle elongated at 1.14 ± 0.07 µm/min (n = 11) during the first 8 min after metaphase confinement and at 1.16 ± 0.07 µm/min (n = 8) in the first 8 min of anaphase B (compared with 0.56 ± 0.08 µm/min [n = 6] in unconfined anaphase) (Figure 1, B–E). Thus mechanisms activated by confinement are sufficient to achieve a similar rate of spindle elongation in metaphase and anaphase cells of the same shape. This suggests that the spindle's elongation potential under confinement is similar in metaphase and anaphase despite different cytoplasmic biochemistries and dramatic reorganization of the central spindle region where antiparallel microtubules overlap. The latter hints that the spindle elongation we observe does not depend on a specific microtubule architecture inside the spindle.

To more stringently test this idea, we asked whether monopolar spindles elongate under confinement. In *S*-trityl-L-cysteine (STLC)-generated monopolar spindles, we observed both spindle pole movement and kinetochore-fiber (k-fiber) elongation (Figure 1, F–H, and Supplemental Video 1). This indicates that features unique to a bipolar spindle architecture, such as antiparallel microtubule overlaps, are not necessary to drive confinement-induced spindle elongation.

Finally, we tested whether pushing forces generated by growing microtubules inside the spindle drive confinement-induced spindle elongation. Indeed, we previously observed that k-fiber plus-end polymerization continues during elongation, while minus-end depolymerization at poles stops (Dumont and Mitchison, 2009a). There, under less severe cell confinement, Taxol prevented confinement-induced pole separation. Here, under more severe confinement, we found that spindle poles separated at a similar rate when k-fiber lengthening was inhibited by Taxol, though they reached a shorter steady-state separation (Figure 1, I and J). As Taxol-treated spindles elongated, the distance between nearest opposing k-fiber plus ends increased to 5.2 ± 0.9 µm (n = 9), whereas in untreated cells, spindle elongation did not affect the interkinetochore distance (n = 11; Dumont and Mitchison, 2009a) (Supplemental Figure S1, A–C). In Taxol, these large distances between opposing k-fiber plus ends suggested that at least one k-fiber detached from each sister kinetochore pair to allow spindle elongation in the absence of k-fiber growth. Coimaging of kinetochore component CenpC with tubulin confirmed rupture of k-fibers from kinetochores (Figure 1K, Supplemental Figure S1D, and Supplemental Video 1). This suggests that k-fiber growth does not drive confinement-induced spindle elongation but rather occurs as a result of this phenomenon.

Together these data suggest that forces outside—rather than inside—the spindle change under confinement to drive spindle elongation. This is consistent with changes in astral microtubule forces driving spindle elongation under confinement.

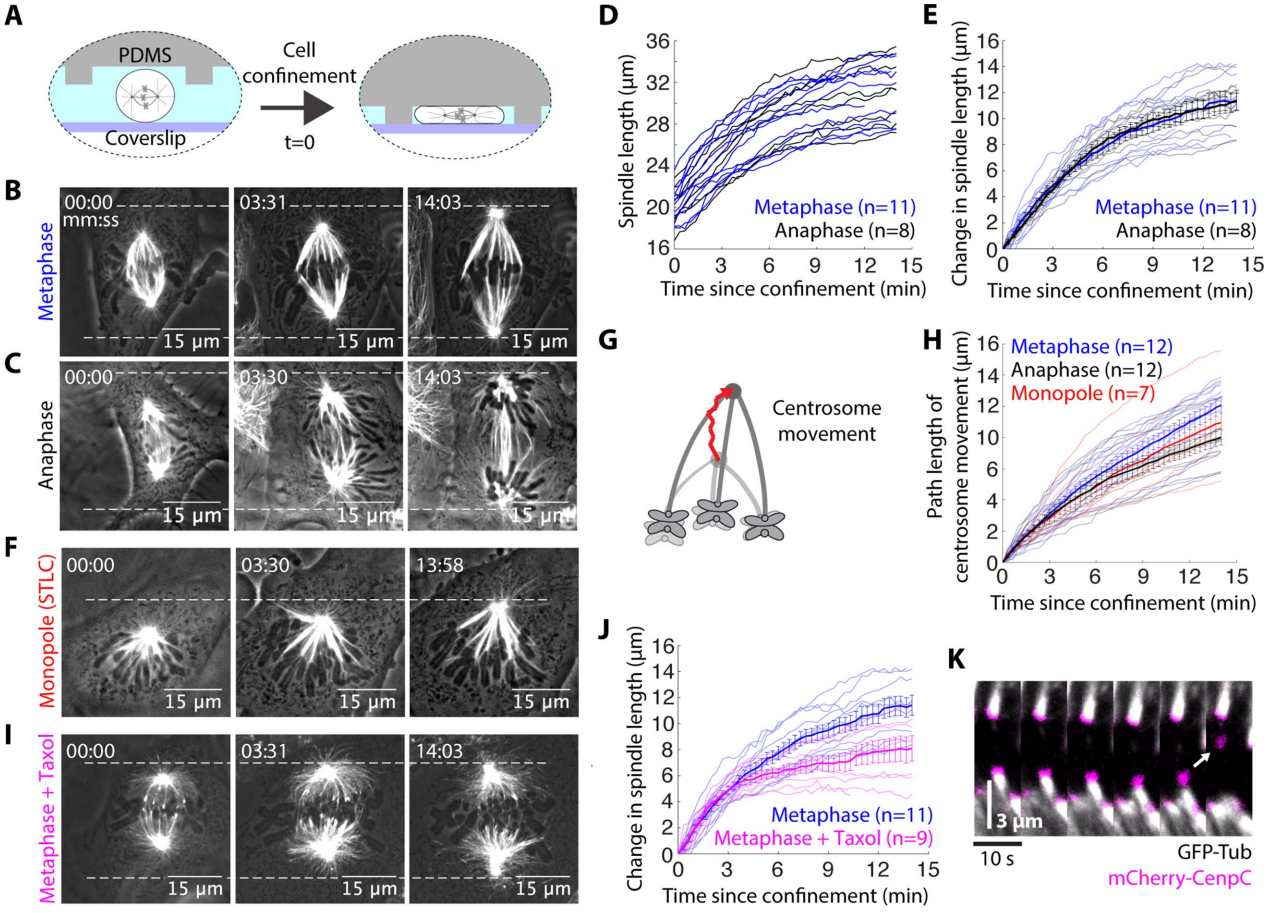

FIGURE 1: Metaphase, anaphase, monopolar, and Taxol-stabilized spindles elongate at similar rates when confined. (A) Schematic diagram of PDMS-based cell confinement. (B, C) Confocal images of representative examples of (B) confinement-induced metaphase spindle elongation and (C) anaphase B spindle elongation in a confined cell. (D) Metaphase and anaphase spindle length following confinement. (E) Mean ± SEM (thick line) and individual traces (thin lines) of change in spindle length for metaphase and anaphase spindles following confinement. (F) Representative example of confinement-induced (STLC-induced, 10 µM) monopolar spindle elongation. (G) Schematic and (H) mean ± SEM (thick line) and individual traces (thin lines) of path length of centrosome movement following confinement in metaphase, anaphase, and monopolar spindles. (I) Representative example of confinement-induced Taxol-treated (10 µM) metaphase spindle elongation. (J) Mean ± SEM (thick line) and individual traces (thin lines) of change in spindle length for metaphase and Taxol-treated metaphase spindles following confinement. (K) Example sister kinetochore pair (mCherry-CenpC) demonstrating that k-fibers (GFP-tubulin) can fall off kinetochores to allow spindle elongation in Taxol. For B, C, F, and I, phase-contrast and GFP-tubulin images are merged. For all data, PtK2 GFP-tubulin cells were captured by confocal imaging and confinement occurs at $t = 0$ and persists thereafter.

Cell confinement promotes lateral microtubule growth at the cell cortex

On the basis of simple geometric arguments, we hypothesized that cell shape changes, and thus confinement, alter the distribution of contact geometries between astral microtubules and the cell cortex, and that this drives spindle elongation. To test this hypothesis, we asked whether both natural and confinement-induced variations in cell shape correlated with different contact geometries of astral microtubules with the cortex. In particular, it has been suggested that decreased distance between the centrosome and the cell cortices facilitates lateral astral microtubule growth events (Samora *et al.*, 2011), which may allow application of additional sliding forces by cortical motors to lengthen the spindle.

We first harnessed the natural diversity in cell shapes to determine whether decreased distance between the centrosome and cell cortex correlates with increased lateral microtubule growth in PtK2 green fluorescent protein (GFP)-tubulin cells. We found that the number of astral microtubules visible along their length in the cell's lowest confocal imaging plane increased in cells with centrosomes nearer the lower cell cortex (Figure 2, A and B). Furthermore, spindle length was greater (19.7 ± 0.6 µm, $n = 17$) in cells in which centrosomes were near (2–3 µm) the lower cortex, than in cells in which centrosomes were far (4–5 µm) from the lower cell cortex (15.4 ± 0.2 µm, $n = 13$) (Figure 2C). We also noticed that the distance between the centrosomes and the lower cell cortex increased as cell height increased (correlation coefficient = 0.76; $p < 0.001$, $n = 29$). Thus a shorter cortex-to-centrosome distance and a lower cell height correlates with increased lateral astral microtubule-to-cortex contacts in unconfined cells, and outward force on spindle poles may scale with the extent of lateral microtubule-to-cortex contact.

To probe whether this is also true in confined cells, we imaged PtK2 GFP-tubulin cells three-dimensionally before and after confinement. Before confinement, in the lowest in-focus confocal plane,

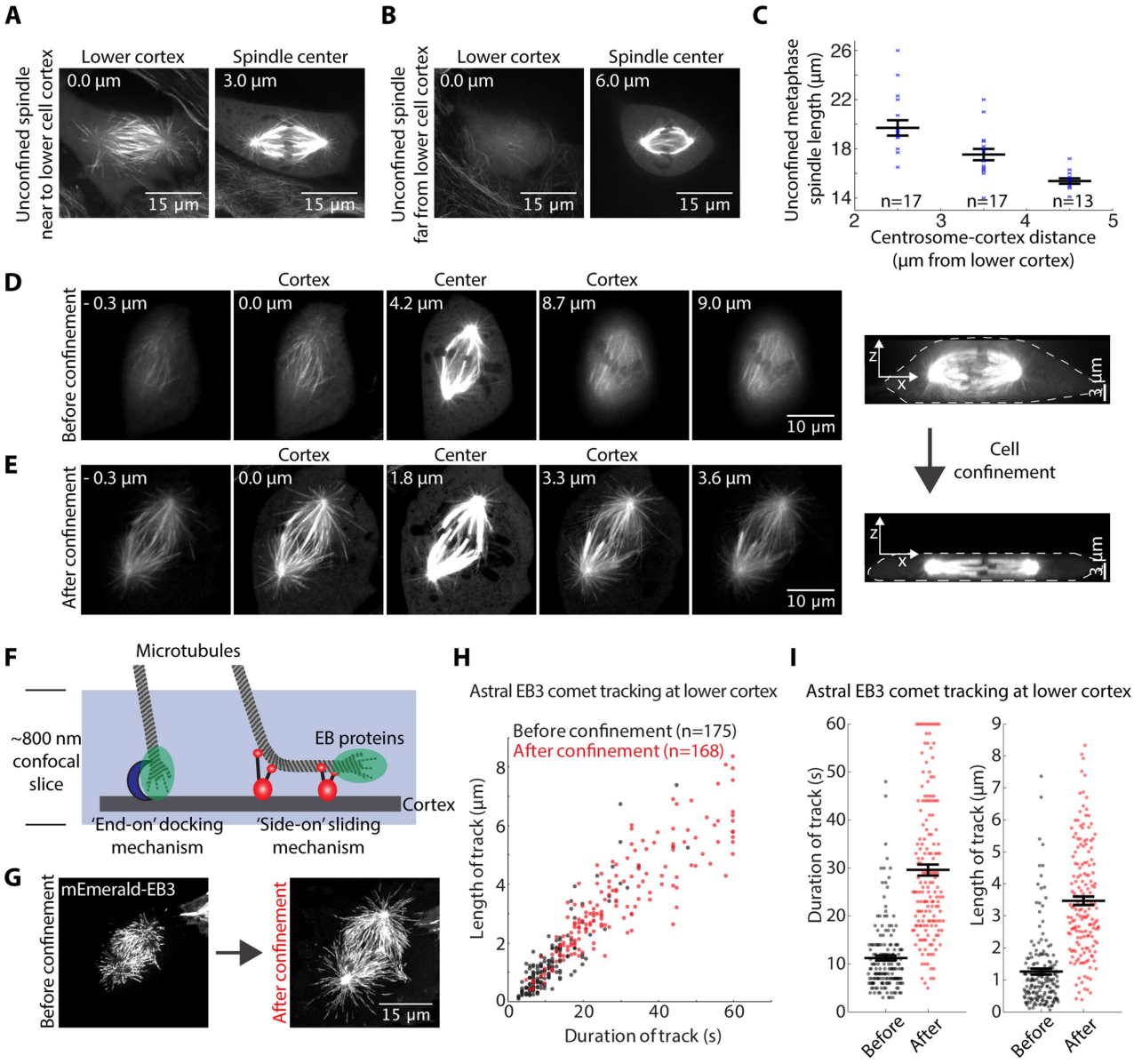

FIGURE 2: Confinement promotes lateral microtubule growth at the cell cortex. (A, B) Confocal images of the lower cortex (0 µm) and spindle center (distance from cortex noted in micrometers) in unconfined PtK2 GFP-tubulin metaphase cells with (A) a "long" spindle nearer the cortex and (B) a "short" spindle farther from the cortex. (C) Unconfined metaphase spindle length (mean ± SEM) correlates with distance of centrosomes to the lower cell cortex. (D, E) Confocal z-stacks of the same PtK2 GFP-tubulin metaphase spindle (D) before and (E) after confinement (with lower cortex at 0 µm, and upper cortex distance noted). (F) Schematic demonstrating alternative force-generating mechanisms and microtubule contact geometries at the cell cortex during mitosis. (G) mEmerald-EB3 maximum-intensity projection (from confocal images) over time at the lower cell cortex for a 1 min period before and after metaphase cell confinement. (H) Length and duration of EB3 comet tracks at the lower cell cortex ($n = 4$ cells analyzed both before and shortly after confinement). (I) Duration and length of comet tracks (mean ± SEM) from H are plotted separately to display statistical significance.

only astral microtubule tips were visible, suggesting end-on contacts (Figure 2D). Following confinement, however, we observed an increase in lateral astral microtubule growth at the cell cortex (Figure 2E). To track the tips of growing astral microtubules and assess their behavior at the cell cortex, we imaged mEmerald-EB3 in the lowest confocal plane (Figure 2F). During a 1 min window, EB3 comet tracks increased in duration from 11.2 ± 0.5 s ($n = 175$) before confinement to 29.6 ± 1.1 s ($n = 168$) after confinement; meanwhile, the mean length of EB3 comet tracks increased from 1.3 ± 0.1 µm ($n = 175$) to 3.5 ± 0.1 µm ($n = 168$) (Figure 2, G–I). Increased duration and length of trackable plus-end growth events near the cell cortex upon confinement suggests that confinement promotes lateral cortical microtubule attachments and decreases short-lived end-on contacts (Figure 2I). Lateral microtubule attachments could provide the more persistent platforms for cortical force generation required to power spindle elongation.

Force is applied along the length of astral microtubules

Given that confinement promotes lateral microtubule-to-cortex contacts and leads to spindle elongation, increased number and

extent of lateral contacts at the cortex may drive spindle elongation at metaphase. A simple prediction of this model is that lateral cortical astral microtubules are under tension.

To test this, we used laser ablation to detach individual astral microtubules from the spindle and mapped the ensuing microtubule movements (Figure 3, A–C, and Supplemental Video 2). In metaphase PtK2 GFP-tubulin cells in which centrosomes were near the lower cortex, 30 out of 34 severed cortical microtubules slid outward after being severed (max. glide speed: 0.94 ± 0.10 µm/s, $n = 27$). In anaphase, 24 out 28 severed cortical microtubules slid outward after being severed (max. glide speed: 1.10 ± 0.11 µm/s, $n = 22$) (Figure 3D). The similar proportion of gliding events and similar postablation velocities in metaphase and anaphase suggest that force generation by cortical motors is not differentially regulated between these two mitotic stages. Additionally, cortical microtubules in confined cells slid outward postablation at similar rates to those observed in unconfined cells (max. confined metaphase glide speed: 1.17 ± 0.14 µm/s, $n = 6$; max. confined anaphase glide speed: 1.24 ± 0.17 µm/s, $n = 7$) (Supplemental Video 2). Finally, astral microtubules growing along the cortex toward the cell center from the spindle poles also moved in the direction of their plus ends when severed (Figure 3E), suggesting that motors acting on them are not excluded from the central cell cortex. The symmetry breaking that causes increased force on astral microtubules to translate into outward force on centrosomes may arise from asymmetric enrichment of cortical dynein anchors (Kiyomitsu and Cheeseman, 2012) or from the unique fate of astral microtubules that grow into the spindle body.

Released microtubules sometimes buckled against the cell cortex upon reaching the cell edge (Figure 3C). This suggested that force is exerted along the sides of astral microtubules, not just at their plus ends, as these microtubules are still being driven into the cell boundary, even when their plus ends no longer move. To gain insight into how many motors are required to generate sufficient buckling force, we calculated the critical force required to buckle microtubules of the lengths observed. We assumed that the microtubule behaves as a stiff rod under compression, that is, that $F_c = \pi^2(EI/L^2)$, where EI is the flexural rigidity of a microtubule (~2.6 × 10^{-23} N·m^2) and L is the microtubule length (Gittes *et al.*, 1996). We further assumed that the ends of the microtubules are free to rotate, but not move laterally, and considered only microtubules for which lateral movement of the microtubule tip was not observed during buckling. These calculations revealed that forces >10 pN sometimes act on buckling microtubules (Figure 3F; F_c = 6.9 ± 1.2 pN, $n = 21$). This suggests that multiple dynein motors act on a single microtubule, since a single mammalian dynein motor generates 1–2 pN (Mallik *et al.*, 2004; McKenney *et al.*, 2010; Ori-McKenney *et al.*, 2010).

Together these data suggest that a general pulling mechanism that acts along the length of microtubules at the cell cortex is in place at both metaphase and anaphase and is independent of both location within the cell and external confinement.

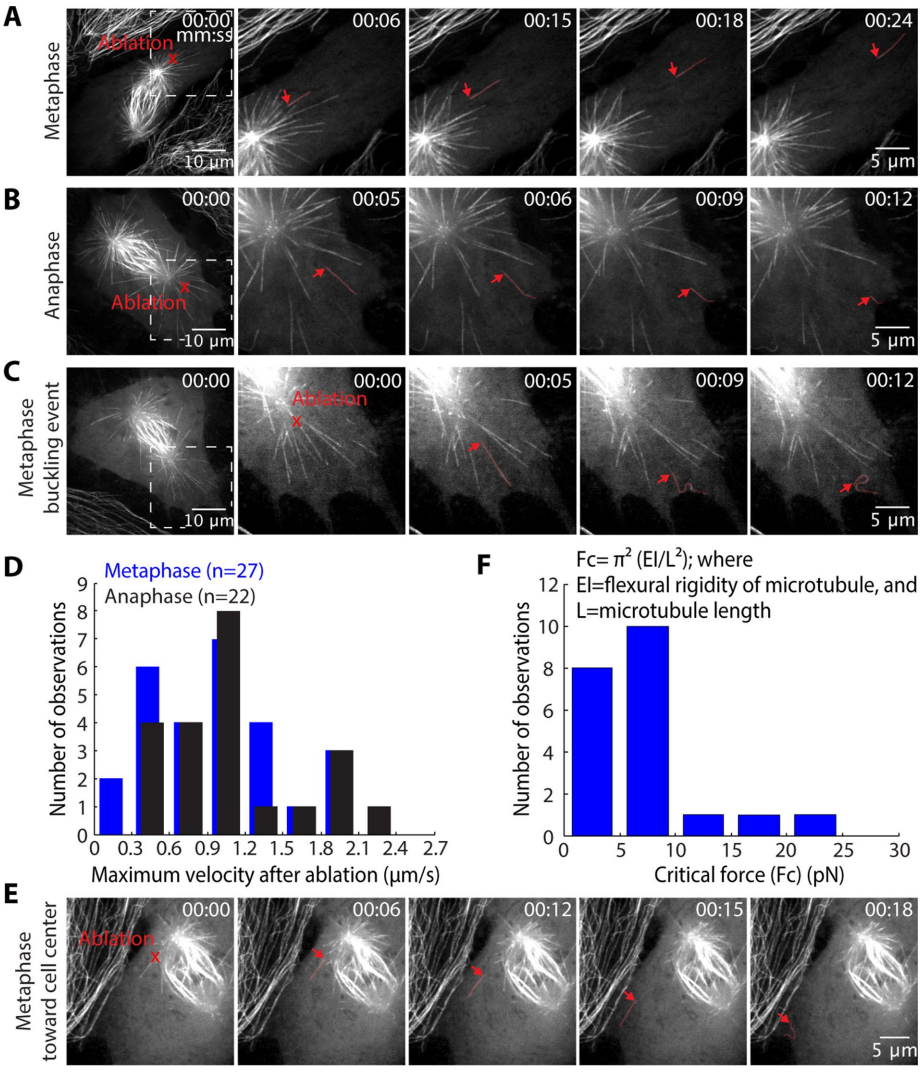

FIGURE 3: Force is applied along the length of astral microtubules at both metaphase and anaphase. Confocal images of (A) metaphase and (B) anaphase unconfined PtK2 GFP-tubulin cells in which laser ablation (red "X") was used to sever astral microtubules near the centrosome at the lower cell cortex. Severed astral microtubules (red) moved away from the spindle. (C) Severed microtubules (red) frequently buckled against the cortex. (D) Histogram of the maximum speed reached by each severed microtubule at metaphase and anaphase (n = number of cuts). (E) In a metaphase cell, an astral microtubule extending into the spindle is pulled toward the cell edge upon detachment from the spindle (ablation at red "X"; arrow points to new minus end). (F) Histogram of calculated critical forces required for observed buckling events at both metaphase and anaphase.

Dynein and astral microtubules are required for confinement-induced spindle elongation

If dynein-mediated cortical sliding force on astral microtubules is responsible for confinement-induced spindle elongation, a central prediction is that elongation should require both dynein activity and astral microtubules. Here we sought to test both of these model predictions.

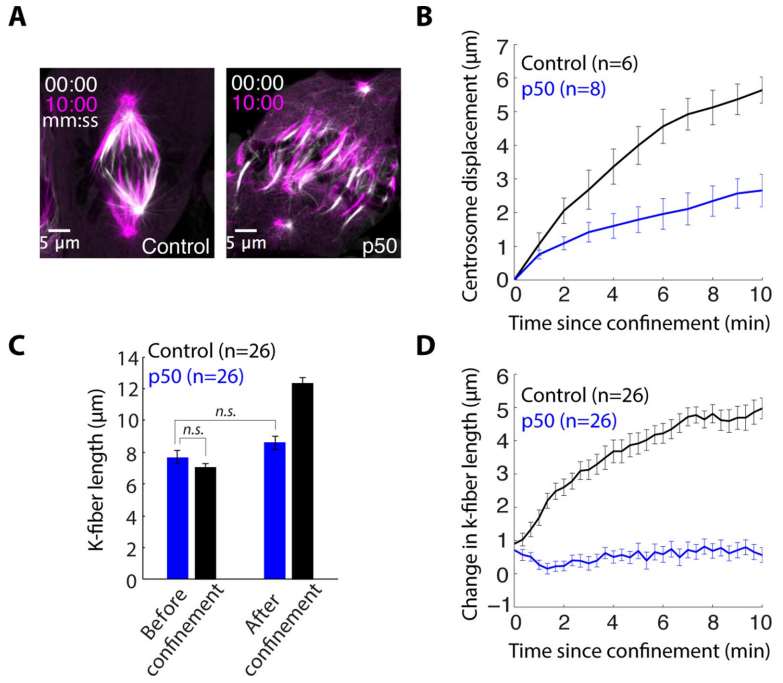

FIGURE 4: Dynein is required for confinement-induced spindle elongation. (A) Confocal images of PtK2 GFP-tubulin cell immediately following confinement (white) and 10 min after confinement (magenta) in a control cell and a cell overexpressing p50 to inhibit dynein. (B) Centrosome displacement (mean ± SEM, *n* = number of centrosomes) from the original position following confinement in control and p50-overexpressing cells. (C) K-fiber length (mean ± SEM, *n* = number of k-fibers) before confinement and 12 min after confinement in p50 overexpression and control cells. (D) Change in k-fiber length (mean ± SEM, *n* = # k-fibers) following confinement in p50-overexpressing and control cells.

To test whether dynein is required for confinement-induced spindle elongation, we inhibited the dynein–dynactin interaction by overexpressing dynamitin (p50) in PtK2 cells (Howell *et al.*, 2001; Melkonian *et al.*, 2007). This resulted in unfocused spindle poles and k-fiber minus ends detached from centrosomes (Figure 4A). Before confinement, average k-fiber length was indistinguishable in p50 overexpression (7.73 ± 2.07 µm, *n* = 26) from control (7.36 ± 1.31 µm, *n* = 26), despite changes in spindle architecture. Following confinement, however, dynein inhibition reduced centrosome displacement and prevented elongation of k-fibers (Figure 4, B–D, and Supplemental Video 3). Thus confinement-induced centrosome movement, and changes in spindle and k-fiber length, depend on dynein-powered force generation and organization.

To test whether astral microtubules are required for this confinement-induced spindle elongation, we first used the Plk4 inhibitor centrinone to inhibit centrosome duplication and make spindles with one centrosome (Wong *et al.*, 2015). The lower GFP-tubulin intensity and fewer astral microtubules at one pole identified the half-spindle without a centrosome (Supplemental Figure S2A). Confinement of one-centrosome spindles resulted in normal pole movement and elongation in the half-spindle with the centrosome and significantly reduced pole movement in the half-spindle without a centrosome (Figure 5, A and B, and Supplemental Video 4). Together these data indicate that the dynein-generated force is applied on astral microtubules to drive confinement-induced spindle elongation. The data also indicate that any other changes potentially induced by confinement, for example, cell volume changes or passive responses to confinement forces, are not sufficient to drive spindle elongation.

We next tested whether sustained force on astral microtubules is necessary to maintain the longer spindle steady state, or whether it is only needed during the elongation process. To do so, we confined PtK2 GFP-tubulin metaphase cells and allowed spindles to elongate and reach their new steady-state lengths and then used laser ablation to abruptly remove one centrosome and reduce associated astral microtubules (Supplemental Figure S2, B and C), from one pole (Khodjakov *et al.*, 2000). Upon centrosome ablation, the associated half-spindle shortened and established a new steady-state length (Figure 5, C and D, and Supplemental Video 4). Meanwhile, the opposite half-spindle, still containing a centrosome, did not shorten over this time period (Figure 5E). Thus centrosome positioning forces can regulate the length of k-fibers attached to that centrosome, independent of the opposite half-spindle. Similarly, the metaphase plate did not move much when the spindle expanded or retracted asymmetrically (Figure 5). We suspect that force can be dissipated by polymerization at kinetochores and without being transmitted to the other half-spindle; thus the spindle center is effectively soft and deformable to pulling forces. Together our results indicate that confinement increases sliding forces generated by dynein at the cell cortex on astral microtubules and that these forces are both sufficient to induce spindle elongation, and necessary for maintenance of the elongated state (Figure 5F).

Regulation of force on astral microtubules provides temporal control of spindle remodeling

In this study, we used confinement-induced metaphase spindle elongation to investigate mechanical and geometric regulators of spindle remodeling. Our work demonstrates that a simple physical change—increasing lateral microtubule contacts at the cortex—is sufficient to trigger mammalian spindle elongation. As such, our work suggests that mitotic rounding, which is nearly ubiquitous in metazoans, could effectively minimize side-on contact. Minimizing side-on contacts may reduce pulling forces and centrosome separation, and thereby allow a metaphase spindle length that permits adequate chromosome capture by microtubules in mitosis (Kirschner and Mitchison, 1986; Domnitz *et al.*, 2012; Lancaster *et al.*, 2013). Furthermore, pulling forces on lateral microtubules tend to decenter the spindle as positive feedback increases lateral contacts as asters approach the cell cortex (Kern *et al.*, 2016). Limiting contact geometry to end-on may allow contributions from alternative mechanisms, such as cytoplasmic pulling or pushing against the cortex, to help ensure a centered metaphase spindle (Kimura and Kimura, 2011; Garzon-Coral *et al.*, 2016). At anaphase, spindle elongation coincides with astral microtubule lengthening and increased lateral contact (Canman *et al.*, 2003; Rusan and Wadsworth, 2005; Kwon *et al.*, 2015), both of which are well suited to trigger greater side-on cortical pulling force (Gibeaux *et al.*, 2017). Together our data suggest that manipulating microtubule-to-cortex contact geometry—whether by promoting or limiting lateral contacts—could provide temporal control of spindle positioning and remodeling.

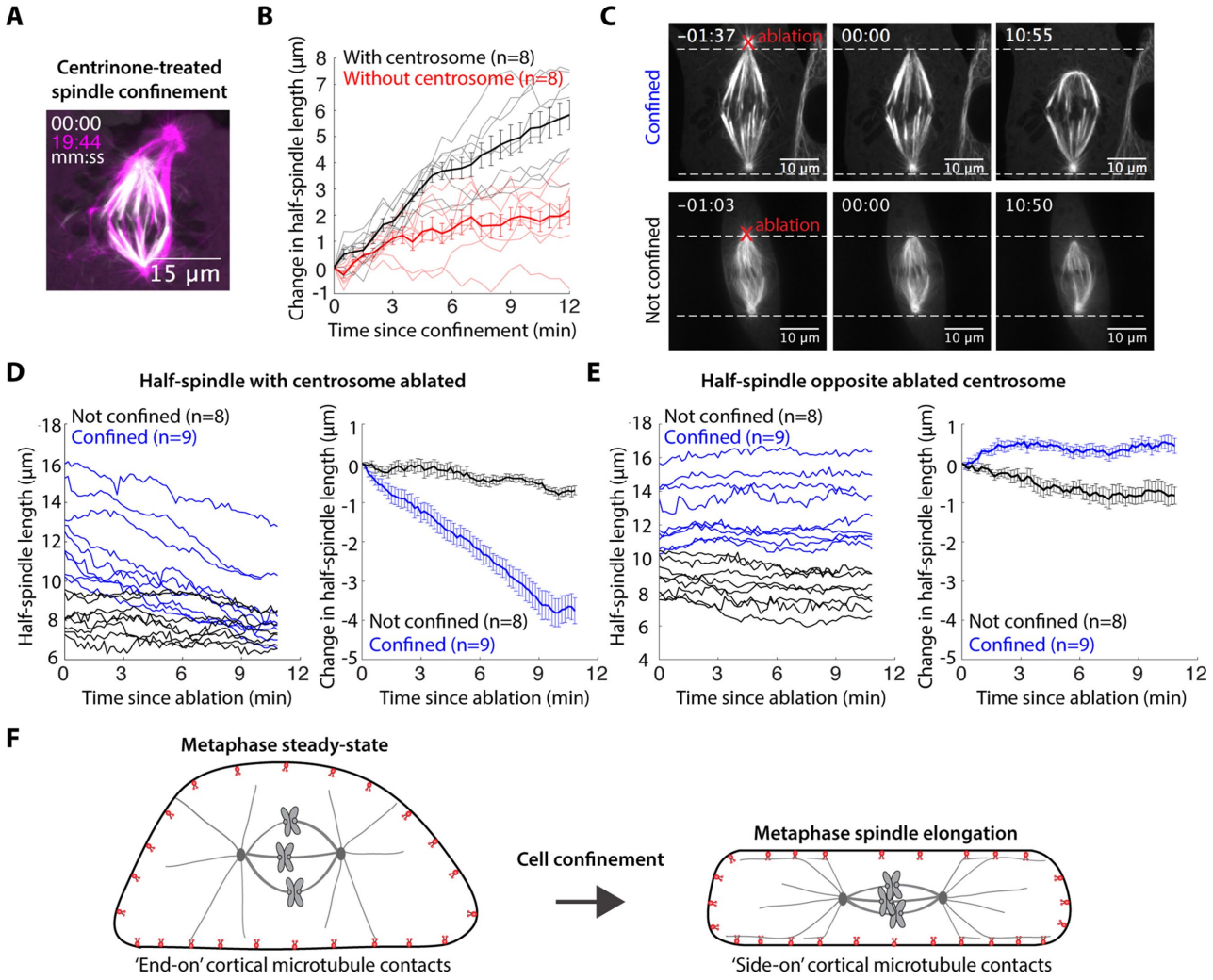

FIGURE 5: Astral microtubules are required for confinement-induced spindle elongation. (A) Confocal images of a centrinone-treated (125 nM) PtK2 GFP-tubulin cell immediately following (white) and almost 20 min after confinement (magenta). (B) Half-spindle elongation (mean ± SEM) following confinement of centrinone-treated cells. Confinement occurs at $t = 0$. (C) Time-lapse confocal images of PtK2 GFP-tubulin cells demonstrating the representative asymmetric response to centrosome ablation (at $t = 0$, red "X") in a cell confined 15 min before ablation (top) and an unconfined (bottom) cell. (D, E) Half-spindle length and changes in half-spindle length (mean ± SEM) following ablation ($t = 0$) in the (D) half-spindle with centrosome ablated at $t = 0$ or (E) half-spindle opposite the ablated centrosome. (F) Model schematic: confinement increases sliding forces generated by dynein at the cell cortex on astral microtubules, and these forces are both sufficient to induce spindle elongation and necessary for maintenance of the elongated state.

Our data provide direct evidence that changes in force outside the spindle drive mammalian spindle elongation under confinement (Figures 1 and 3–5). We had previously presented arguments, based on indirect evidence under milder confinement, that changes in forces inside the spindle likely drove elongation under confinement (Dumont and Mitchison, 2009a). However, we note that our present conclusion is consistent with this previous indirect evidence: First, while spindle poles sometimes elongated faster than centrosomes, poles can have attached astral microtubules independent of centrosomes (Supplemental Video 4). Second, k-fibers sometimes bent during elongation, but this is not necessarily inconsistent with pulling forces on k-fibers. Third, spindle elongation still occurred in latrunculin, but all cortical force generation may not require actin (Redemann *et al.*, 2010). Finally, the present data do not exclude, and may even suggest (Figure 5D), that other mechanisms contribute to spindle elongation.

The data and model (Figure 5F) we provide raise the question of what signals to k-fibers that they should lengthen as the centrosome moves outward. Connections between k-fiber minus ends and moving centrosomes are required for k-fiber lengthening (Figure 4). Dynein itself, pulling on k-fiber minus ends (Elting *et al.*, 2014; Sikirzhytski *et al.*, 2014) while walking along centrosomal microtubules, may translate forces on centrosomes to tension on k-fiber minus ends. This tension could, in turn, lead to the observed decrease in depolymerization at k-fiber minus ends under confinement, and as such to k-fiber elongation. In normal, unconfined spindles, lower pulling forces on centrosomes may lead to k-fibers being under less tension or under compression at poles (Dumont and Mitchison, 2009b). This would explain the observed depolymerizion of k-fiber minus ends in steady-state metaphase spindles. Mechanical force from astral microtubules on centrosomes may tune k-fiber minus-end dynamics, just as mechanical

force at kinetochores tunes k-fiber plus-end dynamics (Franck *et al.*, 2007).

MATERIALS AND METHODS

Cell culture, transfection, and drug treatments

PtK2 cells and PtK2 GFP-α-tubulin cells (a gift from Alexey Khodjakov, Wadsworth Center [Khodjakov *et al.*, 2003]) were cultured in MEM as previously described (Elting *et al.*, 2014). Two or three days before imaging, cells were plated on 35 mm dishes with #1.5 poly-D-lysine–coated coverslips (MatTek) (except cells were plated on 25 mm round #1.5 coverslips coated in poly-L-lysine [Sigma P-1524] for Figure 3). For visualization of microtubule plus ends and kinetochores, PtK2 cells were transfected with GFP-α-tubulin and mEmerald-EB3 (gifts from Michael Davidson, Florida State University), and mCherry-CenpC (a gift from Aaron Straight, Stanford University), using Viafect (Promega). In dynein–dynactin inhibition experiments, PtK2 cells were transfected with GFP-α-tubulin and mCherry-dynamitin (p50) (a gift from Trina Schroer, Johns Hopkins University) using Viafect. Fifteen minutes before imaging, 10 μM STLC (Sigma-Aldrich) was added to induce monopolar spindles. Five to ten minutes before imaging,10 μM Paclitaxel (Sigma-Aldrich) was added to limit microtubule dynamics. Forty-eight hours before imaging,125 nM centrinone (gift from Karen Oegema and Andrew Shiau, Ludwig Institute for Cancer Research) was added to inhibit centrosome duplication.

Cell confinement

To confine cells, a suction cup device was adapted from a previous design using soft-lithography techniques (Le Berre *et al.*, 2012). SU8 was used to photolithographically pattern a negative relief of pillar structures (height: 5 μm; diameter: 200 μm; spacing: 700 μm center to center) with desired height in 10-mm-diameter regions. PDMS (Sylgard 184, SigmaAldrich) was mixed with curing agent and poured over the region at a 10:1 ratio. A 10-mm-diameter coverslip was then pressed onto the pattern and baked at 80°C for 1 h. The coverslip, with micropillar spacers attached, was then peeled away from the mold and attached to the suction cup device. For cell-confinement assays, the device was attached to a milliliter syringe, placed on a coverslip with adherent cells, and attached using negative pressure. After image acquisition was initiated, additional negative pressure was created by hand to lower the pillared coverslip onto cells. Confinement was applied gradually over a period of 30 s to 1 min.

Imaging, laser ablation, and data analysis

Three similar inverted spinning-disk confocal (CSU-X1; Yokogawa Electric Corporation) microscopes (Eclipse TI-E; Nikon) with the following components were used for live-cell imaging: head dichroic Semrock Di01-T405/488/561 (except Di01-T488 for GFP-α-tubulin only), 488 nm (100, 120, or 150 mW) and 561 nm (100 or 150 mW) diode lasers, emission filters ET525/36M (Chroma Technology) for GFP (except ET500LP for GFP-α-tubulin only) or ET630/75M for mCherry, and cameras iXon3, Zyla (Andor Technology), or ORCA-ER (Hamamatsu). For imaging, 250 ms exposures were used for phase contrast and 50–200 ms exposures were used for fluorescence. Cells were imaged at 30°C, 5% CO_2 in a closed, humidity-controlled Tokai Hit PLAM chamber (and in a Okolab chamber for Figure 3). Ablation was done using 551 nm ns-pulsed laser light and a galvo-controlled MicroPoint Laser System (Photonic Instruments) operated through Metamorph. Depolymerization of newly created plus ends confirmed single microtubule cuts, and astral microtubule reduction confirmed centrosome ablation. Feature tracking and spindle architecture measurements were done in Fiji either manually or using MTrackJ (Schindelin *et al.*, 2012). All error bars display mean ± SEM. A Student's *t* test was used to determine statistical significance where indicated.

ACKNOWLEDGMENTS

We thank Alexey Khodjakov for PtK2 GFP-α-tubulin cells; Michael Davidson, Aaron Straight, and Trina Schroer for providing plasmids; and Karen Oegema and Andrew Shiau at the Ludwig Institute for Cancer Research for centrinone. We thank Cade Fox for microfabrication help at the Biomedical Micro and Nanotechnology Core (BMNC) at the University of California, San Francisco, and the Nikon Imaging Center at Harvard Medical School for technical support. We thank Jonathan Kuhn, Andrea Serra Marques, other members of the Dumont lab, Fred Chang, Torsten Wittmann, Carlos Garzon-Coral, Jennifer Waters, and Wendy Salmon for helpful discussions. This work was supported by a Herchel Smith Graduate Fellowship (M.B.G.), National Institutes of Health grants F31CA200277 (C.L.H.), R01GM039565 (T.J.M.), and DP2GM119177 (S.D.), the Searle Scholars Program (S.D.), and the Rita Allen Foundation (S.D.).

REFERENCES

Adames NR, Cooper JA (2000). Microtubule interactions with the cell cortex causing nuclear movements in *Saccharomyces cerevisiae*. J Cell Biol 149, 863–874.

Aist JR, Liang H, Berns MW (1993). Astral and spindle forces in PtK2 cells during anaphase B: a laser microbeam study. J Cell Sci 104, 1207–1216.

Brennan IM, Peters U, Kapoor TM, Straight AF (2007). Polo-like kinase controls vertebrate spindle elongation and cytokinesis. PLoS One 2, e409.

Canman JC, Cameron LA, Maddox PS, Straight A, Tirnauer JS, Mitchison TJ, Fang G, Kapoor TM, Salmon ED (2003). Determining the position of the cell division plane. Nature 424, 1074–1078.

Collins ES, Balchand SK, Faraci JL, Wadsworth P, Lee WL (2012). Cell cycle-regulated cortical dynein/dynactin promotes symmetric cell division by differential pole motion in anaphase. Mol Biol Cell 23, 3380–3390.

Domnitz SB, Wagenbach M, Decarreau J, Wordeman L (2012). MCAK activity at microtubule tips regulates spindle microtubule length to promote robust kinetochore attachment. J Cell Biol 197, 231–237.

Dumont S, Mitchison TJ (2009a). Compression regulates mitotic spindle length by a mechanochemical switch at the poles. Curr Biol 19, 1086–1095.

Dumont S, Mitchison TJ (2009b). Force and length in the mitotic spindle. Curr Biol 19, R749–R761.

Elting MW, Hueschen CL, Udy DB, Dumont S (2014). Force on spindle microtubule minus ends moves chromosomes. J Cell Biol 206, 245–256.

Fink G, Schuchardt I, Colombelli J, Stelzer E, Steinberg G (2006). Dynein-mediated pulling forces drive rapid mitotic spindle elongation in *Ustilago maydis*. EMBO J 25, 4897–4908.

Fink J, Carpi N, Betz T, Betard A, Chebah M, Azioune A, Bornens M, Sykes C, Fetler L, Cuvelier D, Piel M (2011). External forces control mitotic spindle positioning. Nat Cell Biol 13, 771–778.

Franck AD, Powers AF, Gestaut DR, Gonen T, Davis TN, Asbury CL (2007). Tension applied through the Dam1 complex promotes microtubule elongation providing a direct mechanism for length control in mitosis. Nat Cell Biol 9, 832–837.

Garzon-Coral C, Fantana HA, Howard J (2016). A force-generating machinery maintains the spindle at the cell center during mitosis. Science 352, 1124–1127.

Gibeaux R, Politi AZ, Philippsen P, Nedelec F (2017). Mechanism of nuclear movements in a multinucleated cell. Mol Biol Cell 28, 645–660.

Gittes F, Meyhofer E, Baek S, Howard J (1996). Directional loading of the kinesin motor molecule as it buckles a microtubule. Biophys J 70, 418–429.

Grill SW, Gonczy P, Stelzer EH, Hyman AA (2001). Polarity controls forces governing asymmetric spindle positioning in the *Caenorhabditis elegans* embryo. Nature 409, 630–633.

Grill SW, Howard J, Schaffer E, Stelzer EH, Hyman AA (2003). The distribution of active force generators controls mitotic spindle position. Science 301, 518–521.

Gusnowski EM, Srayko M (2011). Visualization of dynein-dependent microtubule gliding at the cell cortex: implications for spindle positioning. J Cell Biol 194, 377–386.
Howell BJ, McEwen BF, Canman JC, Hoffman DB, Farrar EM, Rieder CL, Salmon ED (2001). Cytoplasmic dynein/dynactin drives kinetochore protein transport to the spindle poles and has a role in mitotic spindle checkpoint inactivation. J Cell Biol 155, 1159–1172.
Kern DM, Nicholls PK, Page DC, Cheeseman IM (2016). A mitotic SKAP isoform regulates spindle positioning at astral microtubule plus ends. J Cell Biol 213, 315–328.
Khodjakov A, Cole RW, Oakley BR, Rieder CL (2000). Centrosome-independent mitotic spindle formation in vertebrates. Curr Biol 10, 59–67.
Khodjakov A, Copenagle L, Gordon MB, Compton DA, Kapoor TM (2003). Minus-end capture of preformed kinetochore fibers contributes to spindle morphogenesis. J Cell Biol 160, 671–683.
Kimura K, Kimura A (2011). Intracellular organelles mediate cytoplasmic pulling force for centrosome centration in the *Caenorhabditis elegans* early embryo. Proc Natl Acad Sci USA 108, 137–142.
Kirschner MW, Mitchison T (1986). Microtubule dynamics. Nature 324, 621.
Kiyomitsu T, Cheeseman IM (2012). Chromosome- and spindle-pole-derived signals generate an intrinsic code for spindle position and orientation. Nat Cell Biol 14, 311–317.
Kiyomitsu T, Cheeseman IM (2013). Cortical dynein and asymmetric membrane elongation coordinately position the spindle in anaphase. Cell 154, 391–402.
Kotak S, Busso C, Gonczy P (2012). Cortical dynein is critical for proper spindle positioning in human cells. J Cell Biol 199, 97–110.
Kozlowski C, Srayko M, Nedelec F (2007). Cortical microtubule contacts position the spindle in *C. elegans* embryos. Cell 129, 499–510.
Krueger LE, Wu JC, Tsou MF, Rose LS (2010). LET-99 inhibits lateral posterior pulling forces during asymmetric spindle elongation in *C. elegans* embryos. J Cell Biol 189, 481–495.
Kwon M, Bagonis M, Danuser G, Pellman D (2015). Direct microtubule-binding by myosin-10 orients centrosomes toward retraction fibers and subcortical actin clouds. Dev Cell 34, 323–337.
Laan L, Pavin N, Husson J, Romet-Lemonne G, van Duijn M, Lopez MP, Vale RD, Julicher F, Reck-Peterson SL, Dogterom M (2012). Cortical dynein controls microtubule dynamics to generate pulling forces that position microtubule asters. Cell 148, 502–514.
Labbe JC, McCarthy EK, Goldstein B (2004). The forces that position a mitotic spindle asymmetrically are tethered until after the time of spindle assembly. J Cell Biol 167, 245–256.
Lancaster OM, Le Berre M, Dimitracopoulos A, Bonazzi D, Zlotek-Zlotkiewicz E, Picone R, Duke T, Piel M, Baum B (2013). Mitotic rounding alters cell geometry to ensure efficient bipolar spindle formation. Dev Cell 25, 270–283.
Le Berre M, Aubertin J, Piel M (2012). Fine control of nuclear confinement identifies a threshold deformation leading to lamina rupture and induction of specific genes. Integr Biol (Camb) 4, 1406–1414.
Mallik R, Carter BC, Lex SA, King SJ, Gross SP (2004). Cytoplasmic dynein functions as a gear in response to load. Nature 427, 649–652.
McKenney RJ, Vershinin M, Kunwar A, Vallee RB, Gross SP (2010). LIS1 and NudE induce a persistent dynein force-producing state. Cell 141, 304–314.
Melkonian KA, Maier KC, Godfrey JE, Rodgers M, Schroer TA (2007). Mechanism of dynamitin-mediated disruption of dynactin. J Biol Chem 282, 19355–19364.
Minc N, Burgess D, Chang F (2011). Influence of cell geometry on division-plane positioning. Cell 144, 414–426.
Nguyen-Ngoc T, Afshar K, Gonczy P (2007). Coupling of cortical dynein and G alpha proteins mediates spindle positioning in *Caenorhabditis elegans*. Nat Cell Biol 9, 1294–1302.
O'Connell CB, Wang YL (2000). Mammalian spindle orientation and position respond to changes in cell shape in a dynein-dependent fashion. Mol Biol Cell 11, 1765–1774.
Ori-McKenney KM, Xu J, Gross SP, Vallee RB (2010). A cytoplasmic dynein tail mutation impairs motor processivity. Nat Cell Biol 12, 1228–1234.
O'Rourke SM, Christensen SN, Bowerman B (2010). *Caenorhabditis elegans* EFA-6 limits microtubule growth at the cell cortex. Nat Cell Biol 12, 1235–1241.
Redemann S, Pecreaux J, Goehring NW, Khairy K, Stelzer EH, Hyman AA, Howard J (2010). Membrane invaginations reveal cortical sites that pull on mitotic spindles in one-cell *C. elegans* embryos. PLoS One 5, e12301.
Rusan NM, Wadsworth P (2005). Centrosome fragments and microtubules are transported asymmetrically away from division plane in anaphase. J Cell Biol 168, 21–28.
Samora CP, Mogessie B, Conway L, Ross JL, Straube A, McAinsh AD (2011). MAP4 and CLASP1 operate as a safety mechanism to maintain a stable spindle position in mitosis. Nat Cell Biol 13, 1040–1050.
Schindelin J, Arganda-Carreras I, Frise E, Kaynig V, Longair M, Pietzsch T, Preibisch S, Rueden C, Saalfeld S, Schmid B, *et al.* (2012). Fiji: an open-source platform for biological-image analysis. Nat Methods 9, 676–682.
Sikirzhytski V, Magidson V, Steinman JB, He J, Le Berre M, Tikhonenko I, Ault JG, McEwen BF, Chen JK, Sui H, *et al.* (2014). Direct kinetochore-spindle pole connections are not required for chromosome segregation. J Cell Biol 206, 231–243.
Su KC, Barry Z, Schweizer N, Maiato H, Bathe M, Cheeseman IM (2016). A regulatory switch alters chromosome motions at the metaphase-to-anaphase transition. Cell Rep 17, 1728–1738.
Thery M, Jimenez-Dalmaroni A, Racine V, Bornens M, Julicher F (2007). Experimental and theoretical study of mitotic spindle orientation. Nature 447, 493–496.
Tsou MF, Ku W, Hayashi A, Rose LS (2003). PAR-dependent and geometry-dependent mechanisms of spindle positioning. J Cell Biol 160, 845–855.
Wong YL, Anzola JV, Davis RL, Yoon M, Motamedi A, Kroll A, Seo CP, Hsia JE, Kim SK, Mitchell JW, *et al.* (2015). Reversible centriole depletion with an inhibitor of Polo-like kinase 4. Science 348, 1155–1160.
Wu H, Nazockdast E, Yu C, Shelley MJ, Needleman DJ (2016). Biophysics of mitotic spindle positioning in *C. elegans* embryos. Mol Biol Cell 27, 3947 (P1878).
Wuhr M, Tan ES, Parker SK, Detrich HW III, Mitchison TJ (2010). A model for cleavage plane determination in early amphibian and fish embryos. Curr Biol 20, 2040–2045.
Zhang D, Nicklas RB (1996). "Anaphase" and cytokinesis in the absence of chromosomes. Nature 382, 466–468.